(NASA-CR-126246) INVESTIGATION OF THE FRACTURE MECHANICS OF BORIDE COMPOSITES Quarterly Report L.A. Kaufman (Manlabs, Inc.) Jan. 1972 32 p CSCL 11D

N72-21555

Unclas
G3/18 22399



MATERIALS RESEARCH AND DEVELOPMENT

MANLABS, INC.
21 ERIE STREET
CAMBRIDGE
MASS. 02139

CAT. 18

Quarterly Report No. 5

# INVESTIGATION OF THE FRACTURE MECHANICS OF BORIDE COMPOSITES

Contract No. NASW - 2088

Submitted to:

NASA Headquarters
Washington, D.C. 20548

Attention: Mr. James Gangler

January 1972

## I. INTRODUCTION AND BACKGROUND

The study of fracture characteristics of diboride composites has from the outset been divided into two parts: studies of fracture energies based upon results of impact and slow bend tests of notched specimens and studies of material development designed to produce diboride composites with improved fracture characteristics relative to the diboride materials developed by the Air Force for lifting reentry applications (1,2). In the first year of the program effort was expended in both areas. Impact tests and slow bend tests were conducted for nine (9) diboride composite materials and for high strength WC6Co which was employed as a control material. The immediate object of the material development program was to produce a diboride composite with impact and slow bend fracture energies comparable to the levels displayed by WC6Co, 0.76 ft. lbs. for the standard sized notched impact specimen. The latter value is equivalent to 73.9 in. lbs/in$^2$ (12950 J/M$^2$). Diboride composites containing $ZrB_2$ as the principal phase with one or more of the following: SiC to enhance oxidation resistance, carbon to lower the elastic modulus and increase thermal shock resistance, varius metals to attempt to form a ductile intergranular phase, and filaments or fibers to produce a strength reinforcement displayed impact energies from 17 to 28 in lbs/in$^2$ (2978 to 4906 J/M$^2$). Values of fracture energy per unit area were also obtained from slow bend tests of notched specimens which were 2.6 in lbs/in$^2$ (455 J/M$^2$) for WC6Co and 0.40 to 1.30 in lbs/in$^2$ (70 to 227 J/M$^2$) for the boride composites. The data and results of the first year's study are presented in a technical report (3).

During the second year of study, the program has included the processing of boride composites with metal additives employed to lower fabrication temperatures and the measurement of fracture energies as above. The processing studies have a two-fold objective: one to directly produce a strengthened material with improved fracture characteristics and two, to identify a ceramic system which will densify at a reasonably low temperature and to which a suitable reinforcement can be added such that the

composite therby produced will be characterized by improved fracture energies. In the previous progress report (4) it was shown that additions of metallic iron and titanium to zirconium diboride in amounts of twenty and thirty weight per cent reduced fabrication temperatures to 2500° - 2600°F. Impact test data for the metal-diboride composites did not show any trend toward improved material fracture characteristics, however, fracture energies obtained from slow bend test data did. Additional impact test data were provided for undersized specimens of WC6Co, Boride V, and Boride VIII-M2; the results support the accuracy of the impact test procedure (4). The agreement of fracture energies per unit surface are in good agreement for the impact strength levels which characterize the boride composites tested to date. The agreement for the higher strength WC6Co control material is less satisfactory.

During the past quarter fabrication studies were performed with metal additions to zirconium diboride to effect the identification of minimum processing temperatures. Attempts were made to produce wire mesh reinforced zirconium diboride materials using nichrome and stainless steel wire mesh and a $ZrB_2$/Ni matrix. Experiments were also performed with a $ZrB_2$/Zr composition which produced material with a metallic grain boundary phase, Zr, and a $ZrB_2$ matrix phase. Experiments were continued with $ZrB_2$/Ti and $ZrB_2$/Fe compositions. The former additive appears to effect a lowering of processing temperatures by solid state reactions and produce a dense material containing $ZrB_2$ as the principal phase.

Mechanical property tests performed in fracture studies during the past quarter included conventional fracture stress measurement in 4 point bending, slow bend fracture energy measurements using notched specimens in 3 point bending, and impact tests with notched specimens. The results show that $ZrB_2$ 20 Ti can have fracture stress levels approaching 100,000 psi while $ZrB_2$ 20 Zr and $ZrB_2$ 12.5 Ti are characterized by fracture stress levels of 75,000 psi. Fracture surface energies obtained from slow bend tests

of notched specimens of $ZrB_2$ 20 Zr are of the order of 1.15 in lbs/in$^2$ (201 J/M$^2$) Impact data obtained for the $ZrB_2$ metal composite are of the same magnitude as obtained earlier (3) for the ceramic boride compositions, 17 to 28 in lbs/in$^2$ (2978 to 4906 J/M$^2$). The highest values of fracture energy were obtained for $ZrB_2$ 20Ti, 2.10 in lbs/in$^2$ (368 J/M$^2$) but as with the $ZrB_2$/Zr composites, no improvement in impact strength was measured for the tests employed.

## II. FABRICATION AND CHARACTERIZATION

### A. Introduction

The processing studies are designed to produce boride composites for the fracture mechanics investigation. Specimen material is also obtained from commercial suppliers and from billets of boride compositions developed in earlier program (1). The objective of the processing studies is to identify compositions containing $ZrB_2$ as the principal phase and additives which alone or in a particular combination effect (1) lowering of the processing temperature to the vicinity of 2500°F and strengthening or reinforcement such that impact strength and fracture energies are increased relative to the levels of the diboride materials developed earlier (1).

During the current contract year, the processing studies have centered on the use of Fe, Ni, Ti, and Zr as metal additives which have been shown to effectively lower processing temperatures. The Ni-$ZrB_2$ system permits densification at temperatures of 2420°F with the formation of $Ni_3B_4$ as an intermetallic grain boundary phase. The $ZrB_2$/Ni system has been employed together with nichrome and stainless steel wire mesh to attempt to produce reinforced materials with increased impact strength and fracture energies.

### B. Processing and Characterization

Hot pressing experiments were performed with $ZrB_2$ and the following metals each employed as a single additive: Fe, Ti, and Zr. Processing conditions for hot pressing runs completed with Ti and Zr as additives are provided in Table 1. The date for HP 116, HP118, and HP 113 were reported in the last progress report (4). and are repeated in Table 1 for comparison with the new data on Ti and Zr. An additional processing run, HP 129, was completed with $ZrB_2$20Fe, using a hot pressing cycle slightly different from the earlier reported conditions for HP 106 (4).

The earlier hot pressing runs with additions of 12.5 per cent Ti, HP 116 and HP 118, and 20 per cent HP 113, showed that a reduction in processing temperature could be effected and that the two levels of Ti addition produced

different microstructures (4). As discussed in the following section, the impact strength level of the $ZrB_2$20Ti (HP 113) was not significantly different from that reported earlier for the nine diboride compositions (3). However, the fracture energy values obtained from the slow bend tests of specimens from the HP 113 billet were somewhat scattered but the averaged result, 1.27 in/lbs $in^2$ (222 $J/M^2$) was higher than any obtained then for a boride material. During the past quarter, a second billet of $ZrB_2$20Ti was processed for additional fracture studies, HP124, and the Ti addition composition was modified to attempt to consolidate a $ZrB_2$/SiC composition in the same temperature range near 2600°F which is 1000°F lower than that required for the densification of the $ZrB_2$/SiC compositions developed by ManLabs for the U.S. Air Force (1). The billet density results in Table 1 show that the second billet of $ZrB_2$20Ti (100) was successfully densified, HP124. The designation Ti (100) identifies a particular Ti powder lot, United Mineral and Chemical Co, -100 Mesh, commercial Ti powder. The results in Table 1 also show that the addition of SiC to the $ZrB_2$/Ti composition changes the densification characteristics such that the desired fully dense material is not obtained at the 2650°F processing temperature. The SiC addition is desirable as this compound is known to effect increased oxidation resistance for $ZrB_2$ compositions (1). The microstructural features of dense $ZrB_2$20Ti composition is shown at 1500 X magnification in Figures 1 and 2 in the etched condition for HP113 and HP124. The microstructure for HP113 shown in the last progress report (4) was photographed using oblique lighting. The significanc e of the microstructures will be detailed in the next quarter. The X-ray diffraction pattern obtained earlier (4) for HP 113 is consistent with the presence of $ZrB_2$, TiB, and Ti, the latter two phases in lesser amounts than $ZrB_2$. The chemical role of the metallic additive Ti in the immediate discussion, and Ni, Fe, and Zr in subsequent discussions, will be more fully investigated in the next quarter.

The use of metallic Zr as an additive for $ZrB_2$ was selected on the basis of the Zr-B diagram shown in Figure 3 which was taken from Rudy's compilation (5). The latter reference work also contains considerable data on ternary systems including Ti-Zr-B which is being employed in the rationalization of the hot pressing results of this system in Table 1. The Zr - B binary

phase diagram shows that solid Zr is in equilibrious with solid $ZrB_2$ up to a eutectic at 1660°C (3020°F). The two hot pressing runs were carried out at maximum processing temperatures of 2900°F (HP126) and 2820°F (HP 139). The majority of hot pressing runs conducted for this program were designed to produce dense billets of 3 inches diameter by 1 inch high. The first run employing elemental Zr was designed to produce a billet of 1/2 inch height while the second was designed for the full 1 inch. The microstructural features of the dense material produced in runs HP126 and HP139 are provided in Figures 4 and 5. X-ray diffraction data for the former are consistent with the presence of $ZrB_2$ as the principal phase and Zr. The microstructure suggests that liquid phase formation was imminent if not present to some degree. Mechanical property data presented in the following section are consistent with the presence of a grain boundary strengthening agent.

Data and results on the hot pressing of $ZrB_2$/Fe compositions presented in the last progress report (4) showed that the Fe additive was equally effective as Ti and Zr in lower the processing temperature. The $ZrB_2$20Fe composition was processed to near full density at a maximum hot pressing temperature of 2820°F. As with the $ZrB_2$/Ti composition, the impact data did not show any pronounced improvement relative to the $ZrB_2$/SiC compositions. However, the fracture energies obtained from slow bend tests were 0.874 in lbs/in$^2$ (153 J/M$^2$), less than those measured for Zr20Ti but higher than those measured for $ZrB_2$/SiC. Accordingly, a second billet of $ZrB_2$20Fe was processed to generate more data on the fracture characteristics of this compositions. A billet was prepared in HP129 for the $ZrB_2$20Fe composition using a new lot of commercial Fe powder (Hoeganaes Lot 87). The billet was hot pressed to full density 6.34 g/cc with a maximum temperature of 2750°F. Examination of the top and bottom surfaces after removal of exterior skin showed a number of cracks over both surfaces. Several cuts were made to expose the interior of the billet and the cracking was observed on surfaces perpendicular to the top and bottom. This billet was rejected for further consideration at this time.

Other processing experiments were performed in attempts to fabricate a metal reinforced $ZrB_2$ material using nichrome and stainless steel wire mesh as the reinforcement and $ZrB_2$20Ni as the matrix. The experimental conditions

employed and the characteristics observed for the resulting billets are provided in Table 2. The matrix phase was selected on the basis of the low processing temperatures required to effect densification; the reinforcements, on the basis of anticipated chemical compatibility and retained mechanical integrity. The latter aspect is supported in part in the reported retention of ductility in nichrome wire mesh in hot pressed reinforced alumina (6).

The processing cycles, HP127, HP131 and HP134 were performed at decreasing maximum hot pressing temperatures using nichrome wire mesh (20 mesh 0.016 in. dia. wire) as the potential reinforcement. The overall result is a chemical degradation of the reinforcement due to reaction with the matrix system. The same result was obtained for HP138 in the attempt to use a stainless steel wire mesh (20 mesh -0.016 in. dia. wire). The nature of the chemical interaction has not been studied in detail but will be pursued in the next quarter when the overall chemistry of the reacting Metal/$ZrB_2$ systems are reviewed. The microstructural features of the materials produced in the attempted hot pressing of the wire reinforced $ZrB_2$20Ni are provided in Figures 6 and 8 through 10. The principal feature of the microstructures is the presence of the grain boundary phase which appears to have wetted the $ZrB_2$ grains.

A similar type of microstructural feature was observed for hot pressed $ZrB_2$20Ni with no reinforcement, HP 90, Figure 7. However, the relative amounts of the grain boundary phase appears to be larger in the microstructures of the $ZrB_2$20Ni/Reinforcement billets shown in Figures 6 and 8 through 10 than in HP 90 with no reinforcement. This observation is consistent with the apparent reactions of the reinforcements with the $ZrB_2$20Ni matrix.

C. Future Considerations

During the next quarter the chemical aspect of the role of several metal additives will be studies in detail to more fully understand the observed phenomena and increase the probability of identifying a suitable reinforcement.

## III. MECHANICAL TEST DATA

### A. Introduction

Mechanical test data provided in the recent technical report (3) for diboride composites included fracture strength for unnotched specimens, fracture energy per unit surface area for notched specimens, and impact energy for notched specimens. The results in the above report showed that a high strength WC6Co cutting tool material has an impact fracture energy of 73.9 in. lbs/in$^2$ (12950 J/M$^2$) and a slow bend fracture energy of 2.6 in lbs/in$^2$ (455 J/M$^2$). Nine boride composites were tested and the impact fracture energies ranged from 17 to 28 in lbs/in$^2$ (2978 to 4906 J/M$^2$) while the slow bend fracture energies ranged from 0.40 to 1.30 in lbs/in$^2$ (70 to 231 J/M$^2$). The significantly large difference between the fracture energies obtained from impact and slow bend tests was noted (3) in contrast to a two-fold difference obtained from impact and slow bend fracture energies measured for ultra high strength steels and titanium alloys (6). Mechanical test data obtained during the second year of this study are of the same types. Materials studied included new hot pressed compositions of $ZrB_2$20Fe, $ZrB_2$30Fe, $ZrB_2$12.5Ti, $ZrB_2$20 Ti $ZrB_2$20Zr and diboride material VIII (18, 10). The latter is an oxidation resistant composition containing $ZrB_2$, SiC and C which was developed by ManLabs (1).

The quantity designated in this study as fracture energy is obtained in two ways. In one procedure it is calculated directly from the impact strength, normalized for the surface area of the specimen directly below the V-notch. The area of one such surface is combined with the impact energy producing the impact fracture energy in units of in lbs/in$^2$ (joules/meter$^2$). In the second procedure a specimen of identical geometry is subjected to a constant rate of load in three point bending until fracture occurs. The specimen deformation is measured as a function of load on a recording strip chart. The work of fracture is obtained from an analysis of the area under the curve. The slow bend fracture energy is normalized to unit surface area by combination with the area of specimen under the V-notch using the same procedure as employed in the impact test data analysis. Fracture studies of brittle materials have employed the general scheme of notched specimens tested in three-point

bending to measure surface energies and related quantities (7, 8, 9). These works present detailed studies of testing procedures and data analyses using familiar brittle materials of low surface energies such as plate glass and magnesia as well as for graphite, poly (methylmethacrylate), and some metallic materials. In the present study the principal reason for conducting selected fracture tests is to ascertain the extent of material improvement for different compositions and processing conditions. The impact test is a particularly stringent test for ceramics but one that is considered significant as particular ceramics approach the status of engineering materials. The slow bend tests were designed to shed additional light on fracture characteristics. In the studies of fracture mechanics cited above, certain testing specifications are prescribed to provide data suitable for particular analyses. It was not within the scope of this program to perform such analyses. The method of data reduction used to date was described in the earlier technical report (3) where it was shown that a clear differentiation could be measured between a known "tough" ceramic material, WC6Co, and the boride compositions such as the $ZrB_2$/SiC composition designated Material V. The slow bend fracture energies obtained for the boride and tungsten carbide materials cover the range from 0.40 in lbs/in$^2$ (70 J/M$^2$) to 2.6 in lbs/in$^2$ (455 J/M$^2$), respectively. The impact data also provided a measurable differentiation between boride materials and WC6Co, 17 in lbs/in$^2$ (2978 J/M$^2$) versus 74 in lbs/in$^2$ (12,950 J/M$^2$).

B. Test Data and Results

The machining of suitable test specimens for several of the $ZrB_2$ Metal compositions was hindered somewhat by a material tendency for cracking and chipping. The impact and slow bend tests were conducted using the specimen geometry, testing apparatus and procedures described in the technical report (3). The notched charpy bar configuration for the testing of all materials was 2.165 in. ($5.50 \times 10^{-2}$M) in overall length with an 0.394 in ($1.0 \times 10^{-2}$M) square end configuration. Selected materials were tested with an undersized specimen of reduced thickness, 0.200 in ($5.08 \times 10^{-3}$M) and equal height, 0.394 in ($1.0 \times 10^{-2}$M). The notch for all specimens was machined by electrical discharge techniques. The root of the V-notch has a radius of 0.001 in. ($2.54 \times 10^{-5}$M)

and a depth of 0.080 in. ($2.03 \times 10^{-3}$M). The impact tests were conducted with ManLabs Model CIM 1.24 ft-lb (32.54 J) Impact Tester. This instrument has a read out accurancy of 0.01 in lb ($1.13 \times 10^{-3}$ J). Fracture stress measurements were performed at a constant rate of loading with a BLH Hydraulic Tensile Testing Machine; specimens of 1.75 inch x 0.200 inch x 0.100 inch were tested in bending to fracture with a four point loading fixture. Earlier reported fracture stress levels were obtained in both 3 point and 4 point bending (3) but for brittle materials the 4 point bending is preferred. Several of the metal-$ZrB_2$ compositions were tested to determine the fracture stress levels.

In selecting materials for specimens for the several mechanical tests employed to date in this program, a decision was made to temporarily delay the measurement of impact strength in favor of the slow bend tests which appear to show different behavior for the different compositions containing $ZrB_2$ and a metal additive (4). Although the impact testing was delayed for the latter materials, diboride Material VIII (18, 10) which was developed earlier (1) was characterized for its impact resistance. The microstructural features for this material and other information are provided in Figure 11. The mechanical property data show that the highest strength, strength to elastic modulus ratio, and strength to density ratio were obtained for this composition in the earlier diboride material program (1). Impact test data provided in Table 3 and Table 3MKS show energy levels of the same magnitude as measured earlier in this program for dense polycrystalline diboride compositions (3).

Slow bend test data were measured for Material VIII (18, 10), $ZrB_2$20Zr, $ZrB_2$20 Ti, $ZrB_2$12.5Ti, and two $ZrB_2$10Cr billets, HP99 (d=4.47 g/cc, 74%) and HP103 (d=5.57 g/cc, 93%) which were prepared earlier but not characterized. The test data are provided in Table 4 and Table 4MKS. With the exception of the two billets containing chromium as an additive, the new slow bend test data show an increase in fracture energies relative to earlier data for the dense polycrystalline diborides not containing high carbon contents (3). The new data provide fracture energies from 1.08 to 2.10 in lbs/in$^2$ (189 to 368 J/M$^2$) for the $ZrB_2$/Ti amd the $ZrB_2$/Zr composites. With the exception of the diboride Material VIII (14, 30) compositions which contain 30 volume per cent carbon, earlier slow bend data provided maximum fracture energies of 0.70 in lbs/in$^2$ (123 J/M$^2$). The highest values of fracture energies for boride materials have been obtained for $ZrB_2$20Ti.

The maximum load recorded during the slow bend test is related to the fracture bending strength. In comparing all available slow bend data, the highest values of maximum loads have been obtained with the exception of WC6Co for $ZrB_2$20Ti, 376 pounds. The magnitude of the fracture energies obtained from slow bend tests of the Material VIII (14,30) compositions are calculated from the increased area under the load deflection curves. The maximum load observed during the slow bend tests of Material VIII(14,30) was 224 pounds which is consistent with the known decreased strength and elastic modulus levels for the VIII (14,30) compositions relative to other boride compositions with considerable less carbon.

Fracture strength was measured in 4 point bending for $ZrB_2$20Zr, $ZrB_2$12.5Ti, and $ZrB_2$20Ti. The results are provided in Table 5 and Table 5MKS. The levels of bending strength are somewhat higher than those measured for the stronger diboride materials which contain SiC and/or carbon (1). The highest strengths have been obtained for $ZrB_2$20Ti and the fracture energies calculated from the slow bend tests are the highest for this composition although the impact strengths do not show any improvement.

C. Future Considerations

Additional specimen material for $ZrB_2$20Ti will be obtained to measure a sufficient number of data points to confirm the indicated improvement in fracture energy and bend strength. Mechanical tests for strength, fracture energy and impact energy will be conducted on new billets as they become available but the emphasis for the next quarter is planned for the processing aspects of the program. Particular emphasis will be placed on the chemical aspects of the reactive hot pressing.

## REFERENCES


1. Clougherty, E.V., "Research and Development of Refractory Oxidation Resistant Diborides, Part II, Volume I: Summary", AFML-TR-68-190, Part II, Vol. I, July 1970

2. Kaufman, L., and Nesor, H., "Stability Characterization of Refractory Materials Under High Velocity Atmospherie Flight Conditions, Part I, Volume I: Summary", AFML-TR-69-84, Part I, Vol. I, March 1970

3. Kaufman, L., Clougherty, E.V., and Nesor, H., "Investigation of Fracture Mechanics of Boride Composites" NASA Technical Report - Contract NASW 2088, July 1971

4. "Investigation of Fracture Mechanics of Boride Composites" Quarterly Report No. 5, NASW 2088, November 1971.

5. E. Rudy, "Compendium of Phase Diagram Data", AFML-TR-65-2, Part V, (1969).

6. Kalish, D., and Kulin, S.A., "Thermomechanical Treatments Applied to Ultrahigh Strength Steels", Final Report Contract NO w 66-0142c, NAVAIR, November 1966

7. Nakayama, J., "Direct Measurement of Fracture Energies of Brittle Materials", J. Am. Cer. Soc. 48, 583-587 (1965)

8. Tattersall, H.G. and Tappin, G., "The Work of Fracture and its Measurement in Metals, Ceramics and other Materials," J. Materials Sci. 1, 296-301 (1966)

9. Davidge, R.W. and Tappin, G., "The Effective Surface Energy of Brittle Materials", J. Materials Sci. 3, 165-173 (1968).

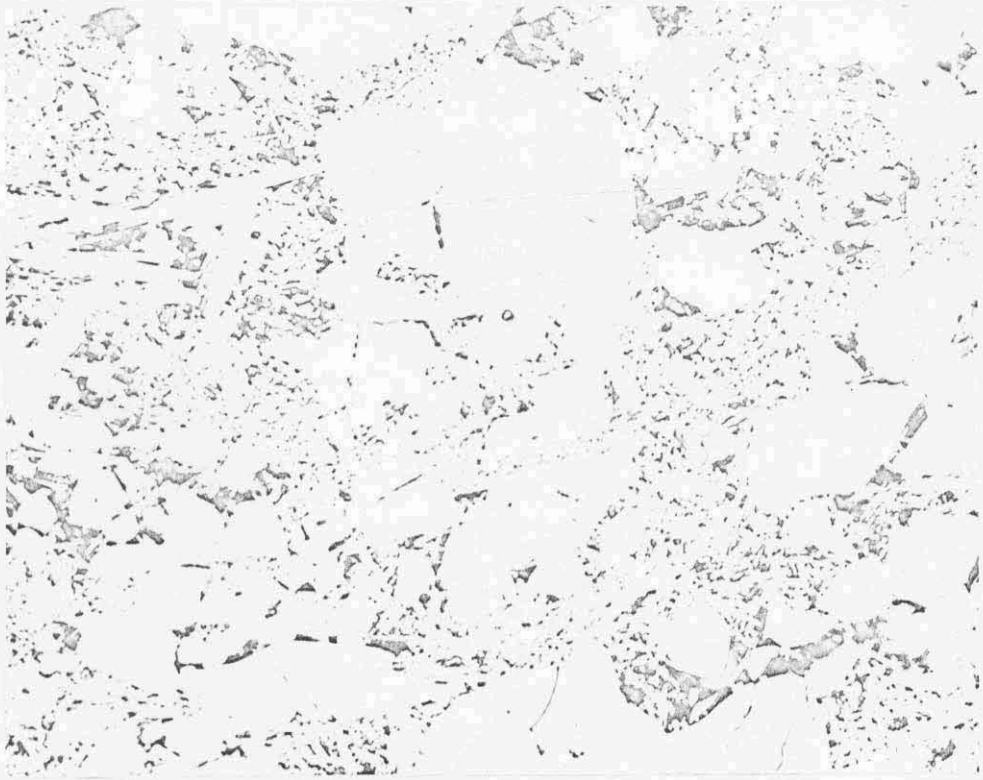

Plate No.
6429

Etched 1500X



Characterization Data:

Density: 5.73 g/cc (100% powder density)

X-Ray Diffraction: $ZrB_2$ principal phase, TiB and Ti identified

Figure 1. Microstructural Features and Characterization Data for Hot Pressed Material $ZrB_2$ 20Ti, HP 113

Plate No. 6419

Etched 1500X



Characterization Data:

| | |
|---|---|
| Density: | 5.6 g/cc |
| X-Ray Diffraction: | $ZrB_2$ principal phase, |

Figure 2 Microstructural Features and Characterization Data for Hot Pressed Material, $ZrB_2$ 20 Ti, HP 124

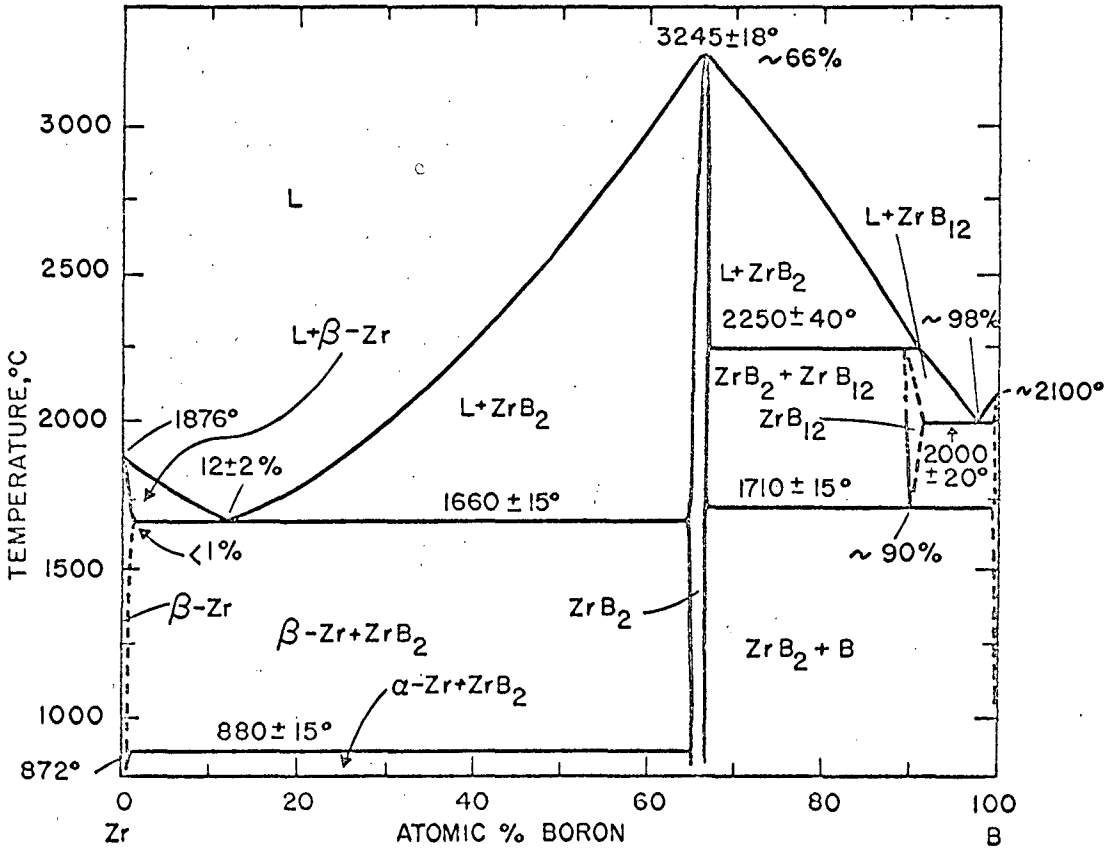


Figure 3. Phase Diagram for Zr-B System (5)

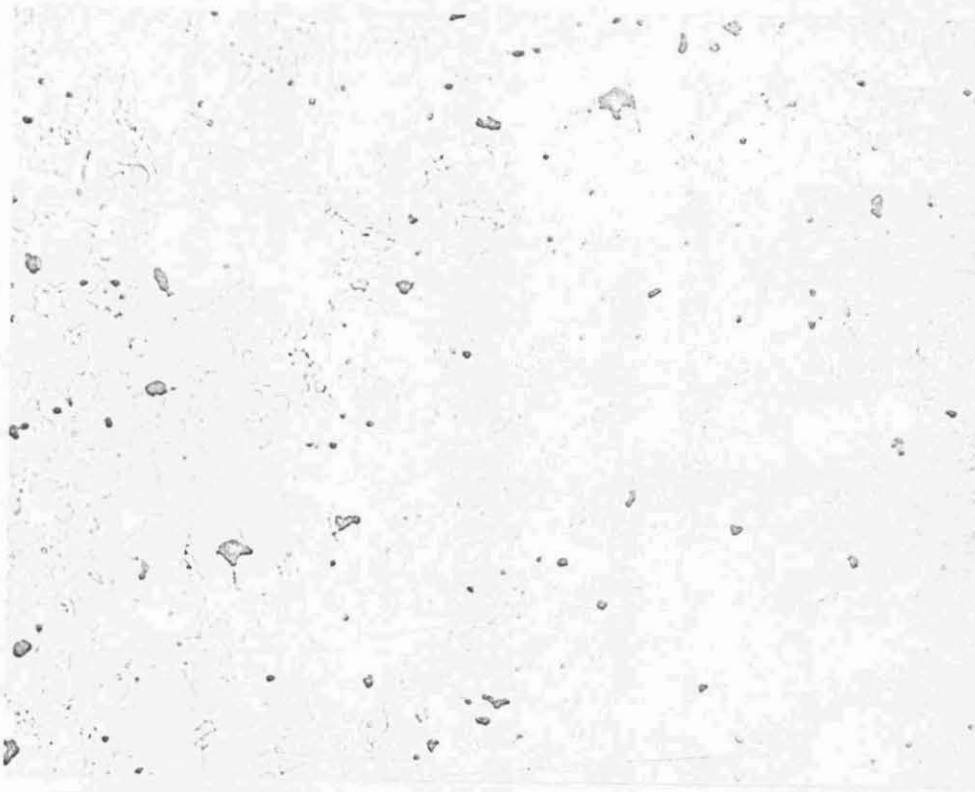

Plate No.
6414A



As Polished 500X

Characterization Data:

Density:

X-Ray Diffraction: $ZrB_2$ principal phase, $\alpha$ Zr identified

Figure 4 Microstructural Features and Characterization Data for Hot Pressed Material, $ZrB_2$ 20Zr, HP 126

Plate No.
6479A

As Polished 500X

Characterization Data:

Density:
X-Ray Diffraction: $ZrB_2$ principal phase, $\alpha$ Zr indentified,
Metallography: Grain Boundary phase observed

Figure 5 Microstructural Features and Characterization Data for Hot Pressed Material, $ZrB_2$ 20Zr, HP 139

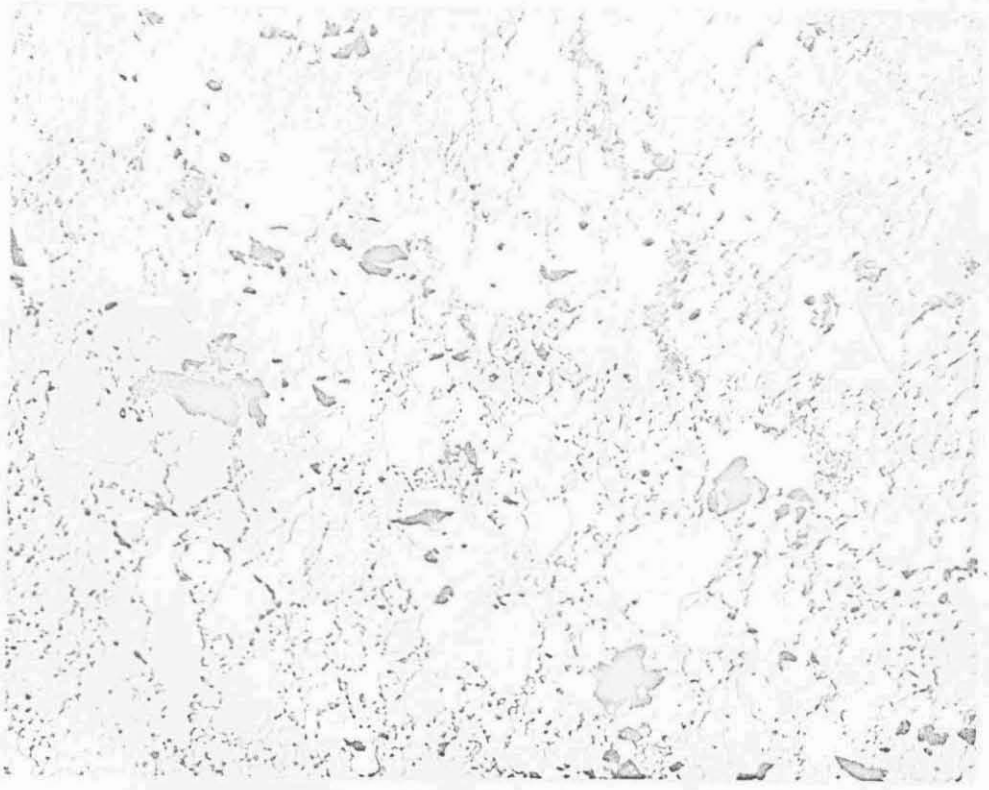

Plate No.
6416

As Polished 500X



Characterization Data

Density:

X-Ray Diffraction: $ZrB_2$ principal phase, $Ni_3B_4$ identified

Metallography: Nichrome reacted leaving voids in otherwise dense microstructure with grain boundary phase observed.

Figure 6 Microstructural Features and Characterization Data for Hot Pressed Material, $ZrB_2$ 20 Ni; Nichrome Wire, HP 127

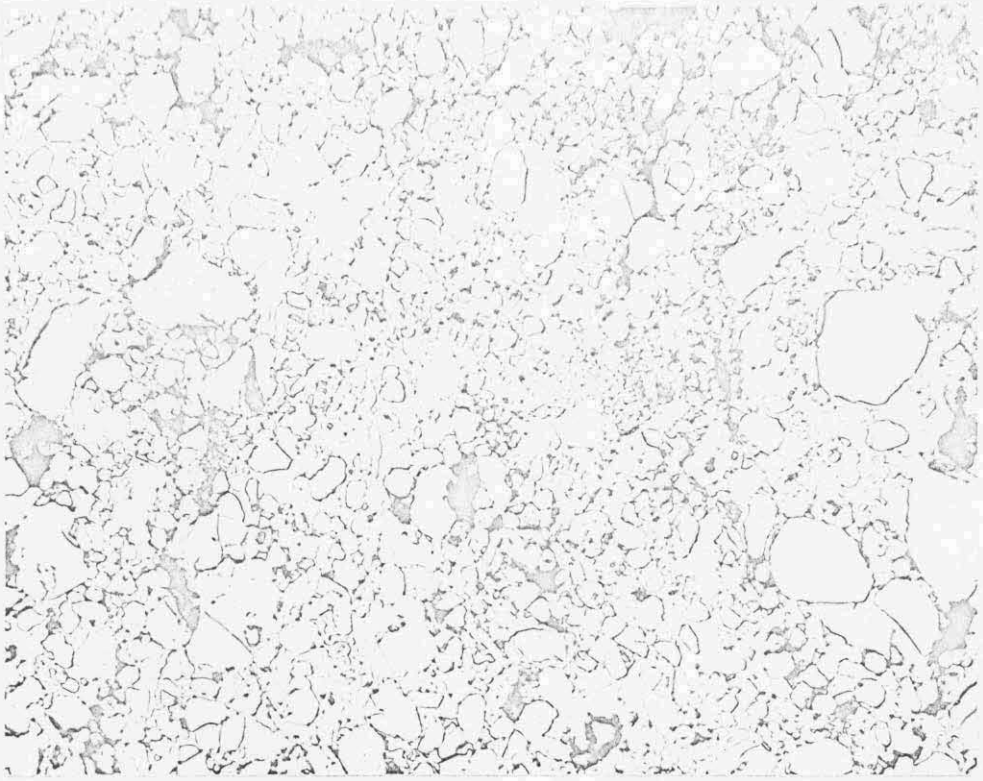

Plate No.
6221

Etched 500X

Characterization Data:

| | |
|---|---|
| Density: | 5.96 g/cc |
| X-Ray Diffraction | $ZrB_2$ principal phase, |
| | $Ni_3 B_4$ type phase identified |

Figure 7 Microstructural Features and Characterization Data for Hot Pressed Material, $ZrB_2$ 20Ni, HP90

Plate No.
6435

As Polished



500X

Characterization Data:

Density:

X-Ray Diffraction: $ZrB_2$ principal phase, $Ni_3B_4$ identified

Metallography: Nichrome reacted leaving voids in otherwise dense microstructure with grain boundary phase observed.

Figure 8 Microstructural Features and Characterization Data for Hot Pressed Material, $ZrB_2$ 20Ni: Nichrome Wire, HP 131

Plate No.
6468

As Polished 500X



Characterization Data:

Density:

X-Ray Diffraction — $ZrB_2$ principal phase, $Ni_3B_4$ identified

Metallography: Nichrome reacted leaving voids in otherwise dense microstructure with grain boundary phase observed

Figure 9 Microstructural Features and Characterization Data for Hot Pressed Material, $ZrB_2$ 20Ni: Nichrome Wire, HP 134

Plate No.
6467

As Polished 500X



Characterization Data:

| | |
|---|---|
| Density: | |
| X-Ray Diffraction | $ZrB_2$ principal phase |
| Metallography: | Stainless steel reacted leaving voids in otherwise dense microstructure with grain boundary phase observed |

Figure 10 Microstructural Features and Characterization Data for Hot Pressed Material, $ZrB_2$ 20Ni: stainless steel wire, HP 138

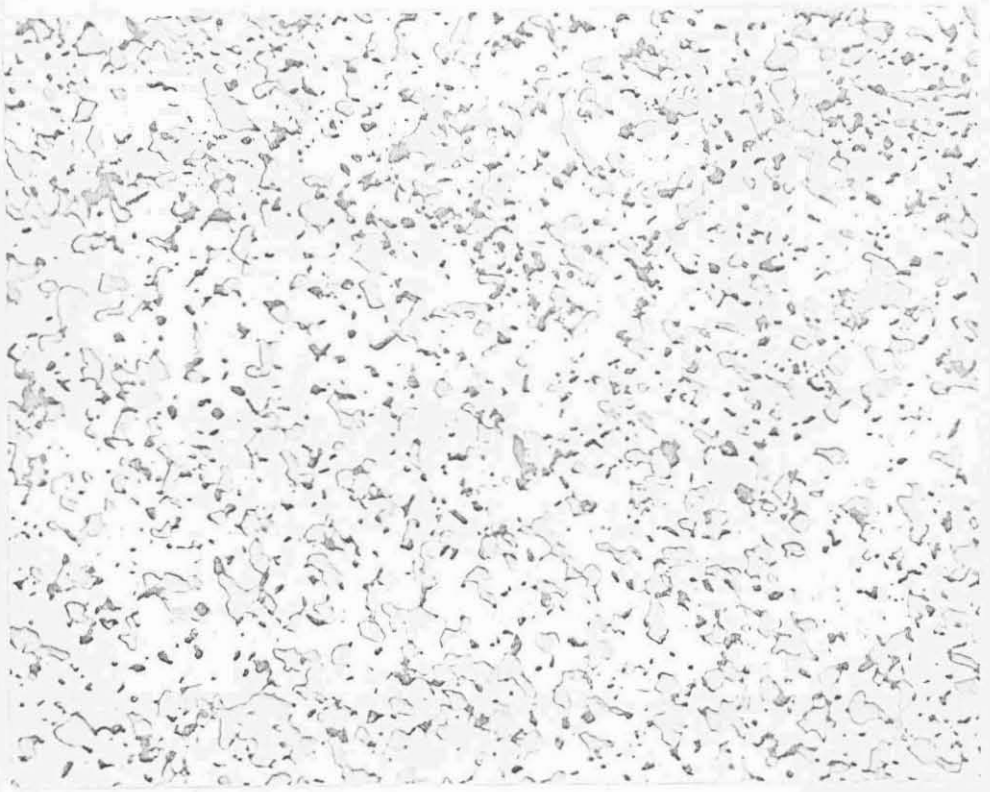

As Polished ManLabs Plate No. 5466 500X

| | |
|---|---|
| Composition: | $72ZrB_2$:18SiC:10C (volume proportions) |
| Billet Identification: | VIII (18, 10) 07F R40L, 5.21 g/cc |
| Billet Size: | 6 inches square by 1.5 inches high |
| Fabrication Conditions: | $3710^{\circ}$ F, 3000 psi, 145 min (at $3710^{\circ}$ F) |
| Billet Density: | 330 lbs/ft$^3$ |

Figure 11 Composition, Fabrication Conditions and Microstructural Features of Diboride Material VIII(18,10).

TABLE 1

Processing Conditions for $ZrB_2$/Ti and $ZrB_2$/Zr Compositions

| Composition* | Billet No. | Processing Conditions** | | | Density | |
|---|---|---|---|---|---|---|
| | | Press | Temp. | Time | Billet | Powder |
| | | psi | °F | min. | g/cc | (%) |
| $ZrB_2$ 12.5 Ti (172) | HP 116 | 3000 | 2500 | 195 | 5.05 | (88.6) |
| $ZrB_2$ 12.5 Ti (172) | HP 118 | 3000 | 2650 | 235 | 5.61 | (98.4) |
| $ZrB_2$ 20 Ti (1198) | HP 113 | 3000 | 2630 | 130 | 5.73 | (100) |
| $ZrB_2$ 20 Ti (100) | HP 124 | 3000 | 2630 | 135 | 5.6 | (99) |
| $ZrB_2$(SiC)20 Ti (100) | HP 122 | 3000 | 2650 | 230 | Low Density | |
| $ZrB_2$ 20 Zr (17127B) | HP 126 | 3000 | 2870-2900 | 87 | | (99) |
| $ZrB_2$ 20 Zr (17127B) | HP 139 | 3000 | 2820 | 145 | | (99) |

*The additive phase is given in weight percent in the starting powder material; the powder lot for the additive phase is identified by the parentheses.

**Conditions cited are the time at the maximum temperature and pressure.

TABLE 2

Processing Conditions for $ZrB_2$/Metal Matrix-Wire Mesh Composites

(3 in. Diameter by 0.5 in Height)

| Compositions* | Billet No. | Processing Conditions** | | | Remarks |
|---|---|---|---|---|---|
| Matrix / Reinforcement | | Press | Temp. | Time | |
| | | psi | °F | min | |
| $ZrB_2$ 20Ni / Nichrome | HP 127 | 3000 | 2420 | 100 | Microstructure dense except for holes |
| | HP 131 | 3000 | 2200 | 215 | ditto |
| | HP 134 | 3000 | 1950 | 115** | Tooling Failed in Heating cycle |
| $ZrB_2$ 20Ni / Stainless | HP 138 | 3000 | 1600-2190 | 165 | Same as 127, 134 |

*The additive phase is given in weight percent in the staring powder material; the powder lot for the additive phase is identified by the parentheses.

**Conditions cited are the time at the maximum temperature and pressure except HP 134 which is total time of run curtailed due mechanical failure of punch during heating cycle.

TABLE 3

IMPACT TEST DATA FOR $ZRB_2$ COMPOSITION: VIII(18,10).

| h | t | Impact Energy | |
|---|---|---|---|
| in. | in. | ft-lbs | in lbs/in$^2$ |
| 0.314 | 0.395 | 0.210 | 20.3 |
| 0.316 | 0.395 | 0.208 | 20.0 |
| 0.314 | 0.395 | 0.289 | 28.0 |
| 0.314 | 0.395 | 0.206 | 20.0 |

TABLE 3 MKS

IMPACT TEST DATA FOR $ZRB_2$ COMPOSITION: VIII(18,10)

| h | t | Impact Energy | |
|---|---|---|---|
| $10^{-3}$ M | $10^{-3}$M | J | J/M$^2$ |
| 7.98 | 10.03 | 0.285 | 3553 |
| 8.03 | 10.03 | 0.282 | 3500 |
| 7.98 | 10.03 | 0.392 | 4900 |
| 7.98 | 10.03 | 0.279 | 3500 |

TABLE 4

Slow Bend Test Data For Diboride VIII (18,10) and $ZrB_2$ Metal Composities
(l = span length = 1.57 in.)

| Spec. No. | h (in) | t (in) | Pmax (lbs) | W (in-lbs) | A ($in^2$) | Fracture Energy W/A (in lbs/$in^2$) |
|---|---|---|---|---|---|---|
| VIII (18,10) R33L | | | | | | |
| A | 0.310 | 0.394 | 223 | 0.116 | 0.122 | 0.95 |
| B | 0.310 | 0.394 | 211 | 0.095 | 0.122 | 0.78 |
| C | 0.315 | 0.393 | 226 | 0.100 | 0.124 | 0.81 |
| D | 0.305 | 0.394 | 225 | 0.116 | 0.120 | 0.97 |
| $ZrB_2$ 20Zr, HP 126 | | | | | | |
| 4 | 0.314 | 0.392 | 270 | 0.153 | 0.123 | 1.24 |
| 3 | 0.320 | 0.392 | 264 | 0.136 | 0.126 | 1.08 |
| $ZrB_2$ 20Ti, HP 124 | | | | | | |
| 1 | 0.318 | 0.395 | 376 | 0.265 | 0.126 | 2.10 |
| 2 | 0.318 | 0.396 | 349 | 0.227 | 0.126 | 1.80 |
| 3 | 0.316 | 0.395 | 277 | 0.160 | 0.126 | 1.27 |
| $ZrB_2$ 12.5 Ti, HP 118 | | | | | | |
| 1 | 0.331 | 0.399 | 287 | 0.161 | 0.132 | 1.22 |
| 4 | 0.331 | 0.399 | 310 | 0.156 | 0.132 | 1.18 |
| $ZrB_2$ 10Cr, HP 99 | | | | | | |
| 1 | 0.314 | 0.393 | 120 | 0.055 | 0.124 | 0.44 |
| 2 | 0.314 | 0.394 | 95 | 0.048 | 0.124 | 0.39 |
| 3 | 0.310 | 0.394 | 117 | 0.047 | 0.122 | 0.39 |
| $ZrB_2$ 10Cr, HP 103 | | | | | | |
| 1 | 0.316 | 0.394 | 122 | 0.040 | 0.125 | 0.32 |
| 2 | 0.316 | 0.394 | 120 | 0.042 | 0.125 | 0.34 |
| 3 | 0.316 | 0.394 | 121 | 0.033 | 0.125 | 0.27 |

TABLE 4 MKS

Slow Bend Test Data For Diboride VIII (18,10) and $ZrB_2$ Metal Composites

(l=span length = 0.0398

| Spec. No. | h $10^{-3}$M | t $10^{-3}$M | Pmax N | W $10^{-3}$J | A $10^{-5}M^2$ | Fracture Energy W/A $J/M^2$ |
|---|---|---|---|---|---|---|
| VIII(18,10)R33L | | | | | | |
| A | 7.87 | 10.00 | 990 | 13.1 | 7.92 | 166 |
| B | 7.87 | 10.00 | 937 | 10.7 | 7.92 | 137 |
| C | 8.00 | 9.98 | 1003 | 11.3 | 8.05 | 142 |
| D | 7.75 | 10.00 | 999 | 13.1 | 7.79 | 170 |
| $ZrB_2$20Zr, HP126 | | | | | | |
| 4 | 7.98 | 9.96 | 1199 | 17.3 | 7.98 | 217 |
| 3 | 8.03 | 9.96 | 1172 | 15.4 | 8.17 | 189 |
| $ZrB_2$20Ti, HP124 | | | | | | |
| 1 | 8.08 | 10.03 | 1669 | 29.9 | 8.17 | 368 |
| | 8.08 | 10.06 | 1550 | 25.6 | 8.17 | 315 |
| 3 | 8.03 | 10.06 | 1230 | 18.0 | 8.17 | 222 |
| $ZrB_2$12.5Ti, HP118 | | | | | | |
| 1 | 8.31 | 10.13 | 1274 | 18.2 | 8.57 | 213 |
| 4 | 8.31 | 10.13 | 1376 | 17.6 | 8.57 | 207 |
| $ZrB_2$10Cr, HP99 | | | | | | |
| 1 | 7.98 | 9.98 | 533 | 6.2 | 8.05 | 77 |
| 2 | 7.98 | 10.00 | 422 | 5.4 | 8.05 | 68 |
| 3 | 7.87 | 9.98 | 519 | 5.3 | 7.92 | 68 |
| $ZrB_2$10Cr, HP103 | | | | | | |
| 1 | 8.03 | 9.98 | 542 | 4.5 | 8.11 | 56 |
| 2 | 8.03 | 9.98 | 532 | 4.7 | 8.11 | 60 |
| 3 | 8.03 | 9.98 | 537 | 3.7 | 8.11 | 47 |

TABLE 5

Fracture Strength Levels for $ZrB_2$ Metal Composites
(4 point bending)

| Material | Bond Strength, $10^3$ psi |
|---|---|
| $ZrB_2$20ZrHP126 | 72.2 |
| | 82.0 |
| $ZrB_2$20ZrHP139 | 76.4 |
| | 78.6 |
| $ZrB_2$12.5TiHP 118 | 76.0 |
| | 78.0 |
| $ZrB_2$20Ti HP124 | 88.0 |
| | 106.5 |

TABLE 5 MKS

Fracture Strength Levels for $ZrB_2$ 1 Metal Composites

(4 point bending)

| Material | Bend Strength, $10^8 N^2/M^2$ |
|---|---|
| $ZrB_2$ 20 Zr HP126 | 4.9 |
| | 5.6 |
| $ZrB_2$ 20 Zr HP139 | 5.2 |
| | 5.3 |
| $ZrB_2$ 12.5Ti HP118 | 5.2 |
| | 5.3 |
| $ZrB_2$ 20 Ti HP124 | 6.0 |
| | 7.2 |